EUROGRAPHICS 2008 / G. Drettakis and R. Scopigno
(Guest Editors)

*Volume 27 (2008), Number 2*

# Accurate Shadows by Depth Complexity Sampling

Vincent Forest, Loïc Barthe and Mathias Paulin†

University of Toulouse, France-IRIT-CNRS

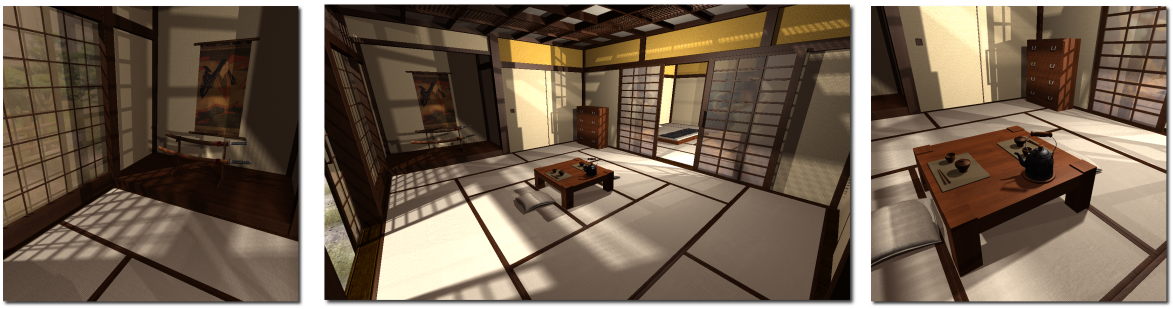

(a) (b) (c)

**Figure 1:** *High quality shadows produced by our algorithm. The* $1024 \times 1024$ *images are computed in* 4 *seconds on a traditional Japanese scene composed of* $501,650$ *triangles, semi-opaque occluders and* 4 *omni-directional area lights.*

**Abstract**

*The accurate generation of soft shadows is a particularly computationally intensive task. In order to reduce rendering time, most real-time and offline applications decorrelate the generation of shadows from the computation of lighting. In addition to such approximations, they generate shadows using some restrictive assumptions only correct in very specific cases, leading to penumbra over-estimation or light-leaking artifacts. In this paper we present an algorithm that produces soft shadows without exhibiting the previous drawbacks. Using a new efficient evaluation of the number of occluders between two points (i.e. the depth complexity) we either modulate direct lighting or numerically solve the rendering equation for direct illumination. Our approach approximates shadows cast by semi-opaque occluders and naturally handles area lights with spatially varying luminance. Furthermore, depending on the desired performance and quality, the resulting shadows are either very close to, or as accurate as, a ray-traced reference. As a result, the presented method is well suited to many domains, ranging from quality-sensitive to performance-critical applications.*

**Keywords:** Soft Shadows, Depth Complexity Sampling, Penumbra Wedge

Categories and Subject Descriptors (according to ACM CCS): I.3.7 [Computer Graphics]: Color, shading, shadowing, and texture

## 1. Introduction

Shadows are fundamental for the realism of virtual 3D scenes. They give information about the relationship between objects and enhance rendering quality by modelling light-surface visibility. Hard shadows are the simplest to generate. Considering the light as a point, they result from the visibility query between a point $\mathbf{p}$ in the scene and the light. If the light is not reduced to a simple point, more realistic soft shadows are produced by evaluating the part of

† {Vincent.Forest, Loic.Barthe, Mathias.Paulin}@irit.fr

the light source visible from **p**. Soft shadows can be seen as a direct extension of hard shadows since they require the evaluation of the visibility query between **p** and an infinite number of samples from the light source. The computation of soft shadows is therefore time-consuming and specific algorithms are required to reduce computational complexity.

For interactive applications, the required real-time frame rate is reached by computing approximated soft shadows. This approximation can be either visually plausible, when it is based on the filtering of hard shadow boundaries [RSC87, Fer05], or physically plausible, when it is computed by evaluating the light area visible from the points **p** seen in the scene [AAM03, GBP06]. However, these last algorithms generate artifacts from overlapping penumbrae, light-leakage and/or have performance bottlenecks. Most of them are based on the shadow maps framework [Wil78]. As a result, they are subject to the artifacts introduced by the discrete, surjective representation of the scene. In addition, their computational complexity and memory consumption increase when they deal with omni-directional lights rather than spot lights. Others are object-based shadow volume algorithms [Cro77]. They do not exhibit the shadow map limitations and despite fill-rate bottleneck and geometry constraints they produce *exact* hard shadows and they naturally handle point, spot and infinite lights.

**Contribution**: Starting from these observations, we take advantage of the robustness of shadow volumes to compute soft shadows as accurately as a ray-traced reference with a controllable, quality-dependent frame-rate ranging from real-time to interactive. In addition, our unified framework provides the required information to correctly solve the rendering equation [Kaj86] for direct illumination from area light sources. Thus, it is well suited for many domains, ranging from quality-sensitive applications to performance-critical ones. Our technique is summarized as follows. For each light, we identify the visible surface points in the penumbra region using the penumbra wedge primitive [AMA02, AAM03]. The depth complexity function returns the number of occluders between *two* points [LAA*05, LLA06]. We evaluate this function between each surface point in the penumbra, and a set of light samples, with a new technique better suited for our real-time requirements. This allows us to directly identify the visible light samples for the surface points, *i.e.* those with a depth complexity equal to *zero*. Then we use this information to either compute the amount of visible light or solve the rendering equation for direct illumination with an accuracy depending on the light sampling.

The remainder of the paper is organized as follows. Section 2 presents a brief overview of previous work on the generation of soft shadows. In section 3, we describe how the depth complexity function is used to compute the amount of light visible from a point **p** according to the opaqueness of the occluder and the luminance of the light samples. The real-time depth complexity computation is detailed in section 4 while section 5 presents the light sampling strategy. In section 6 we show how our approach is used to solve the rendering equation [Kaj86] for direct illumination. Section 7 describes the GPU implementation. Finally, we present results in section 8 and we end with a discussion of directions for future work.

## 2. Related work

Shadow computation is a widely studied problem and a survey on hard shadows has been presented by Woo *et al.* [WPF90], while real-time soft shadows have been recently covered by Hasenfratz *et al.* [HLHS03]. In this section, we focus on the most recent contributions.

Shadow maps [Wil78] have been widely extended to provide soft shadows. Some algorithms use a set of shadow maps per light, limiting their use to static scenes [ARHM00, HBS00, SAPP05]. Others use a single light sample depth map and try to preserve high performance by imposing scene limitations [SS98, BS02] or using heuristics [AHT04, ED06] rather than visibility computations. Recently, Atty *et al.* [AHL*06] and Guennebaud *et al.* [GBP06] introduced soft shadow mapping. In order to compute visibility, they consider the depth map as a discrete representation of the scene and they back-project shadow map samples [DF94] onto the light source. The same concept is presented by Aszódi and Szirmay-Kalos [ASK06] and Bavoil *et al.* [BCS06]. Where the back-projected samples overlap, however, this leads to penumbra over-estimation that can be reduced by a more accurate occluder detection [GBP07] or by a logic binary combination of the back-projected samples [SS07].

Although these algorithms produce convincing results, the inherently discrete, surjective nature of their image-based framework limits their accuracy. This is why, despite the constraints on the occluding geometries, the penumbra wedge algorithm [AMA02, AAM03] is particularly attractive. A penumbra wedge conservatively bounds the penumbra region defined by a silhouette edge seen from the light center. Thus, each point **p** inside a wedge has its light visibility potentially influenced by the corresponding edge. In the penumbra wedge algorithm, the amount of light seen by **p** is computed by the accumulation of the occluded area of the projected silhouette edges onto the light source. However, the overlapping of the back-projected edges leads to over-estimated shadows that can be reduced by an expensive blending heuristic [FBP06].

Laine *et al.* [LAA*05] generalized the penumbra wedge method for *offline* rendering for planar area light sources. In order to compute physically based soft shadows they use the wedges to define a list of edges that can influence the amount of visible light for a point **p**. In a second step, they project the edges, seen from **p**, onto the light source and they use special edge rules to evaluate the depth complexity of

a set of light samples. Finally, to determine whether samples with the lowest depth complexity are occluded, a single shadow ray is cast to one of them. Despite its accuracy, this approach can be less efficient than common ray-traced shadows. Lehtinen *et al.* [LLA06] improve its efficiency and reduce its memory consumption by storing edges in a BSP tree instead of the conservative hemicube data structure. In our approach, neither data structures storing silhouette edges for each **p**, nor explicit edge rules for depth complexity computation, are necessary. In addition, our approach is not limited to planar area light sources and it is well suited to interactive rendering of dynamic scenes.

## 3. From Depth Complexity to Visibility Coefficient

Real-time physically plausible soft shadow algorithms [AAM03, GBP06] decorrelate the generation of shadows from the computation of lighting by defining a *visibility buffer* (v-buffer) storing for each viewed point **p** of the scene its corresponding *visibility coefficient* (v-coef $\in [0,1]$). We denote as v-coef the percentage of visible light and, in this section, we propose a very simple v-coef formulation based on the depth complexity between **p** and a set of light samples.

**Overview:** The *depth complexity function* returns the number of occluders between two points. Considering a light sample **s** and a surface point **p**, **s** is visible from **p** if its depth complexity from **p** is equal to *zero*. Thus, a v-coef for **p** can be simply computed from a set of $N$ samples uniformly distributed over a light $l$ as:

$$V\left(l \leftrightarrow \mathbf{p}\right) = 1 - \frac{1}{N}\sum_{i=0}^{N-1} Sat\left(D\left(\mathbf{s}_{i,l} \leftrightarrow \mathbf{p}\right)\right) \qquad (1)$$

where $D\left(\mathbf{s}_{i,l} \leftrightarrow \mathbf{p}\right)$ returns the depth complexity $\in \mathbb{N}$ between the $i^{th}$ light sample $\mathbf{s}_{i,l}$ and **p**. $Sat\left(x\right)$ is a saturating function that clamps $x$ into $[0,1]$.

**Textured light:** Area light sources such as a fire or a TV screen have a spatially varying luminance. Using depth complexity, such textured light sources can be simply taken into account during the v-coef computation by multiplying the visibility query (*i.e.* the saturated depth complexity) by the sample luminance $L$.

$$V^{rgb}\left(l \leftrightarrow \mathbf{p}\right) = \frac{1}{N}\sum_{i=0}^{N-1} L_{i,l}^{rgb} - L_{i,l}^{rgb} \cdot Sat\left(D\left(\mathbf{s}_{i,l} \leftrightarrow \mathbf{p},\right)\right) \quad (2)$$

The sample luminance can be encoded with an arbitrary color space. However, since the red, green, blue (RGB) representation is well suited for common rendering engines, we define sample luminance and v-coef as RGB values $\in [0,1]^3$. In addition, sample luminance can vary over time. We take into account these animated textured lights by adding time dependence to the luminance.

**Surface opaqueness:** In order to compute soft shadows cast by semi-opaque occluders, we must evaluate the amount of attenuated light from **s** to **p**. This is done by replacing the depth complexity function $D\left(\mathbf{s}_{i,l} \leftrightarrow \mathbf{p}\right)$ in equation 2 by a light attenuation function $Dr\left(\mathbf{s}_{i,l} \leftrightarrow \mathbf{p}\right)$ computed by summing the occluders' percentage of opaqueness. The opaqueness factor is a constant for an occluding surface and it simulates surfacic light attenuation. Functions $D$ and $Dr$ are equal for opaque occluders and in the following, we do not differentiate, instead denoting $D$ and $Dr$ as a real depth complexity function. Note that our surface opaqueness computation is an approximation producing accurate results only when a single semi-opaque surface occludes **p**. Indeed, the light contribution is derived from the sum of opaquess factors while it should rather be modulated by the attenuation factor of *all* occluding surfaces.

## 4. Local Depth Complexity Computation

This section details the streamed evaluation of the depth complexity function. In a first step, we compute the silhouette edges from the entire scene $w$ seen from a light $l$. Then, we initialize the depth complexity between **p** and a set of light samples from the pool of edges $E$ (section 4.1). Finally, the wedges $W$ built from silhouette edges are used to define points **p** whose shadow term is affected by $E$ and to locally update their depth complexity (section 4.2).

### 4.1. Depth Complexity Initialization

The depth complexity between **p** and a light sample **s** was originally defined as the number of surfaces that a ray from **p** to **s** intersects. A depth complexity of $n$ ($n$ greater than *zero*) means that $n$ surfaces occlude **s** as seen from **p**. However, potential changes in the visibility function can occur only on the silhouette edges. It is therefore sufficient to track the occluding silhouette loops rather than the occluding surfaces. In consequence, we reformulate the depth complexity function as the number of silhouette loops occluding **s** from **p**.

This reinterpretation addresses a limitation of previous algorithms. Indeed, as explained by Laine *et al.* [LAA*05], each silhouette edge generates a local change in the depth complexity function and the set of all silhouette edges represents its derivative. Integrating over the local changes results in integrating the derivative of the depth complexity function, and gives the depth complexity without the constant of integration. In order to define this constant, Laine *et al.* cast a shadow ray towards the light sample with the lowest depth complexity, thus limiting the performance and the dynamism of the rendered scene. However, the shadow volume algorithm computes for each visible point **p** the number of occluding silhouette loops. Using the previous reformulation, this defines the constant in the integration of the depth complexity function derivative. As a result we can avoid the

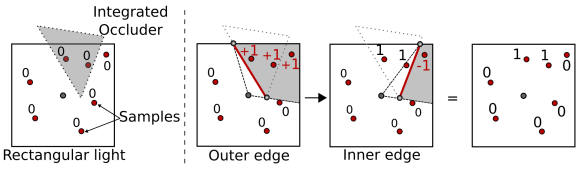


**Figure 2:** *Update of the depth complexity of a set of light samples seen from a point* ***p****. Each occluding edge is projected from* ***p*** *onto the light source. The covered samples are then incremented or decremented according to the wedge type (outer or inner).*

ray casting by initializing the constant of integration with the result of the shadow volume step.

Note that this is quite similar to the initialization step of the penumbra wedge approach [AAM03]. The main difference is that we consider the result of the shadow volume computation as the depth complexity between the light samples and **p** rather than an approximation of its initial v-coef.

### 4.2. Update of the Depth Complexity

**Algorithm 1** update_depth_complexity(Wedges $W$)

```
 1: for all w_e ∈ W do
 2:   for all p in w_e do
 3:     e ← edge associated with w_e;
 4:     e^p ← e projected from p onto the light;
 5:     e^p_c ← e^p clipped against the light border;
 6:     for i = 0 to NBR_LIGHT_SAMPLES − 1 do
 7:       if p.sample[i] is covered by e^p_c then
 8:         if w_e is an outer wedge then
 9:           p.sample[i].depth_complexity += 1;
10:         else
11:           p.sample[i].depth_complexity −= 1;
12:         end if
13:       end if
14:     end for
15:   end for
16: end for
```

The depth complexity integration is performed as in algorithm 1.

The depth complexity between a point **p** and a set of light samples is updated by processing the silhouette edges whose projections from **p** overlaps the light source (line 3). Due to its linear nature, the integration can be performed separately for each projected edge and it is independent for each light sample (line 6). Thus, we update the depth complexity counter independently for each light sample as follows. The shadow volume quadrilateral splits each wedge into two parts: the *inner* part and the *outer* part. In both cases, the edge is projected onto the light source (line 4) to define the covered light samples (line 7). Their corresponding depth complexity counters are then incremented (line 9) or decremented (line 11) if the wedge is respectively outer or inner (figure 2). Since projected edges are clipped (line 5), silhouette edges crossing the light border are also naturally handled (standard offline integrations require specific treatments here).

### 4.3. The Counter Packing

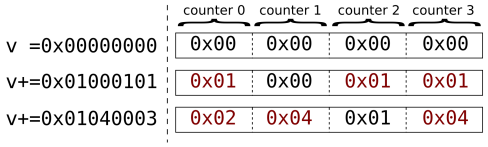


**Figure 3:** *Simultaneous update of four counters* $\in [0..255]$ *packed in a four-byte value. Left: operations on the packed representation; right: resulting value of the packed counters.*

The depth complexity is evaluated with edges encoded as a streamed data set rather than a common static list. Instead of iterating over the list of edges to globally compute the depth complexity between a sample **s** and a point **p**, we progressively update it for each edge that potentially affects the visibility. This avoids the use of a costly pre-computed static space-partitioning data structure referencing silhouette edges [LAA*05, LLA06]. For each visible point **p** we maintain a set of depth complexity counters corresponding to the set of light samples. Therefore the number of available counters must be equal to the number of light samples, and the precision available has to be sufficient to store the maximum number of occluders.

Rendering engines provide render buffers with, typically, *four* values (*red*, *green*, *blue* and *alpha*). In order to provide a sufficient number of counters being both efficiently stored and updated, we pack several counters into a single value as illustrated in the following example. Considering a value $v$ encoded in a 32-bit unsigned integer. The value $v$ can store a single counter ranging from 0 to $2^{32}-1$ or, for instance, *four* values ranging from 0 to 255 in *four* consecutive bytes. This packed representation is particularly well suited for a vectorized incrementation/decrementation. Indeed, assuming that the resulting values do not overflow the domain of the counters, the addition of a *four*-byte value with correctly positioned bits performs a vectorized update of the counters as shown in figure 3.

### 4.4. Advantage and Drawbacks

Counter packing provides an efficient update of the depth complexity counters and increases their quantity. However, only unsigned integers can be used. Even though depth complexity cannot be negative, inner wedges can affect the depth complexity counters before the outer wedges, resulting in

temporary negative values. Thus, we split the depth complexity update into two batches, where outer wedges are treated before the inner ones. Furthermore, semi-opaque occluders require the use of floating point values. We approximate this by discretizing and mapping the opaqueness domain into integers. Note that this limits the precision of both counters and opaqueness.

The depth complexity updates are performed according to the primitives extruded to the silhouette edges and hence, no explicit access to the occluding surfaces is required. However, this precludes the use of surfaces with varying opaqueness.

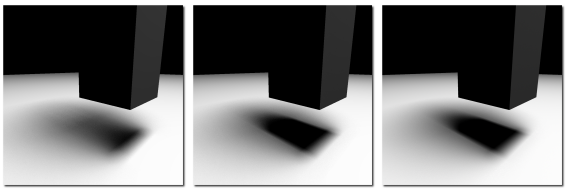

(a) Standard (b) Accurate (c) RT reference

**Figure 4:** *Comparison of silhouette edge determination methods for soft shadows generation. Detecting the silhouette edges from the light center (a) leads to an underestimated penumbra while considering the whole surfacic light (b) avoids this single light sample artifact and produces shadows identical to the ray-traced reference (c).*

Standard silhouette detection from the center of the light leads to the well known single light sample artifact (figure 4(a)). We avoid this using a more accurate approach (figure 4(b)). Considering the planes of two triangles connected to an edge, the edge is a silhouette if a part of the light source is in the positive side of one plane and in the negative side of the other [LAA*05]. Even though this detection is more accurate, note that it generates several silhouette loops where only one is produced by a standard detection. This detection therefore cannot be used on semi-opaque occluders, since the overlapped silhouette loops result in an over-estimated opaqueness factor.

Finally, the presented algorithm generalises the penumbra wedge approach [AAM03] and it can be easily integrated into the penumbra wedge framework.

## 5. Light Sampling Strategy

The quality of the reconstructed visibility function between a point **p** and an extended light source depends on both the number of samples and their distribution over the light (figure 5). In this section we detail our sampling strategy and propose a method to dynamically adjust the balance between the precision of the depth complexity and the number of samples.

### 5.1. Samples Distribution

In order to accurately evaluate the visibility function for **p**, it is necessary to distribute random samples onto the light source using an adapted probability distribution function [PH04]. However, a fixed sampling pattern for all **p** may become visible (figure 5(a)), even with several light samples. In order to alleviate this drawback, one can vary the set of samples for each **p** by randomly rotating the initial sampling pattern (figure 5(b)). In addition to this decorrelation, we perform a better distribution of the samples using a stratified sampling strategy. (figures 5(c) and 5(e)).

### 5.2. Interleaved Sampling

Correlated samples generate visible sampling patterns and their decorrelation generates noise. Interleaved sampling [KH01] takes advantage of both distributions. The main idea is that for neighbour points, a measured signal may produce the same result. Thus, the signal for nearby points is sampled with an interleaved sampling distribution and finally merged into a single sampling pattern. Segovia *et al.* [SIMP06] proposed a real-time framework for this technique. To conserve the coherence between neighbour pixels, they split the rendered image into sub-buffers containing the pixels that use the same distribution of samples. After sampling the desired signal, they gather the sub-buffers and filter the result according to the normal and depth discontinuities.

Interleaved sampling can be efficiently used in our framework (figure 5(d) and 5(f)). However, in order to avoid multiple rendering of shadow volumes and wedges, we use neither the image splitting nor the gather step. In spite of the loss of near points coherence, no drop of performance occurs since no coherent memory access is required (section 7).

### 5.3. Adaptive Sampling

The maximum depth complexity of the rendered scene depends on the scene complexity and the point of view. While rendering a plain leads to a globally low depth complexity, a forest rendering generates many occlusions. Given a fixed amount of available memory for a visible point **p**, we propose a simple way to dynamically adjust the precision and the number of packed depth complexity counters.

The maximum depth complexity between the light samples and **p** is equal to the maximum number of occluding silhouette loops. Thus, in a first step, we track the maximum integration constant $m_c$ resulting from the depth complexity initialization of the current visible points. Then we use this value to define the counter packing encoding. As an illustration, consider the previous example where $four$-byte are available for each visible point. With $m_c$ in $[256, 65535]$, $two$ counters of $two$-byte ($\in [0, 65535]$) can be packed without overflow, while $m_c$ in $[128, 255]$ allows the use of $four$ counters of $one$ byte ($\in [0, 255]$).

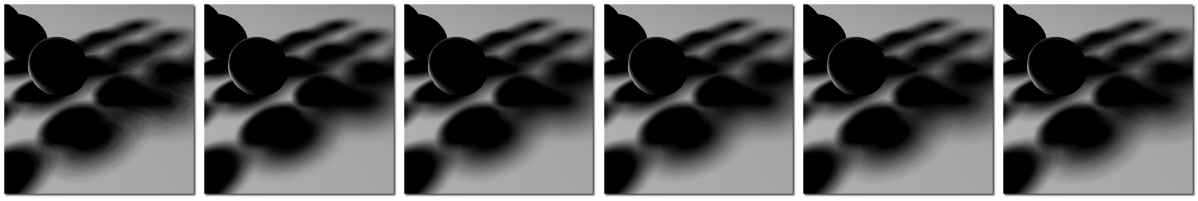

(a) 64 correlated (b) 64 decorrelated (c) 64 stratified (d) 64 interleaved (e) 16 stratified (f) 16 interleaved

**Figure 5:** *Comparison of the soft shadow quality according to the number of samples and the sampling strategy. Shadows are generated with either* 64 *(a, b, c, d) or* 16 *(e, f) samples using a correlated (a), decorrelated (b), decorrelated and stratified (c, e) or interleaved sampling pattern (d, f).*

## 6. Sampling of the Direct Illumination

The depth complexity function is used to compute a *visibility coefficient* of a point $\mathbf{p}$. The v-coef is then used to modulate the direct illumination of $\mathbf{p}$ computed from the center of the light. Hence, considering a set of $j$ lights, the direct illumination according to a given point of view $x\prime$ is computed as:

$$L(\mathbf{p} \rightarrow x\prime) = L_e(\mathbf{p} \rightarrow x\prime) + \sum_j f_s(x \rightarrow \mathbf{p} \rightarrow x\prime) L(x \rightarrow \mathbf{p}) V(l_x \leftrightarrow \mathbf{p}) \frac{cos\theta_o cos\theta_i}{||x-\mathbf{p}||^2} \quad (3)$$

where $L_e$ is the emitted radiance and $f_s$ is the *BSDF*. Even though the visibility is evaluated for an area light source, the direct lighting is still computed using point lights. In order to compute an accurate *direct* illumination for extended light sources, we have to solve the rendering equation [Kaj86] for the surfaces $S$ of the area light sources:

$$L(\mathbf{p} \rightarrow x\prime) = L_e(\mathbf{p} \rightarrow x\prime) + \int_S f_s(x \rightarrow \mathbf{p} \rightarrow x\prime) L(x \rightarrow \mathbf{p}) \upsilon(x \leftrightarrow \mathbf{p}) \frac{cos\theta_o cos\theta_i}{||x-\mathbf{p}||^2} dA(x) \quad (4)$$

Note that the binary visibility $\upsilon(x \leftrightarrow \mathbf{p})$ can be very simply evaluated from the depth complexity function as:

$$\upsilon(x \leftrightarrow \mathbf{p}) = H(D(x \leftrightarrow \mathbf{p})) \quad (5)$$

where $H(x)$ is the Heaviside function that returns *one* if $x$ is strictly positive and *zero* otherwise. Thus, we can numerically solve the equation 4 for the direct illumination, using a set of $N$ samples uniformly distributed over each extended light source, and their corresponding depth complexity:

$$L(\mathbf{p} \rightarrow x\prime) = L_e(\mathbf{p} \rightarrow x\prime) + \sum_j \frac{A(l_j)}{N} \sum_{k=0}^{N-1} f_s(x_{k,j} \rightarrow \mathbf{p} \rightarrow x\prime) L(x_{k,j} \rightarrow \mathbf{p}) H(D(x_{k,j} \leftrightarrow \mathbf{p})) \frac{cos\theta_o cos\theta_i}{||x-\mathbf{p}||^2} \quad (6)$$

where $x_{k,j}$ is the $k^{th}$ sample of the light $j$ and $A(l_j)$ is the area of the $j^{th}$ light source. This equation 6 naturally handles textured lights since the incoming radiance $L(x_{k,j} \rightarrow \mathbf{p})$ of the light samples is explicitly defined. Note that we replace the Heaviside function by the Saturate one when simulating semi-opaque occluders.

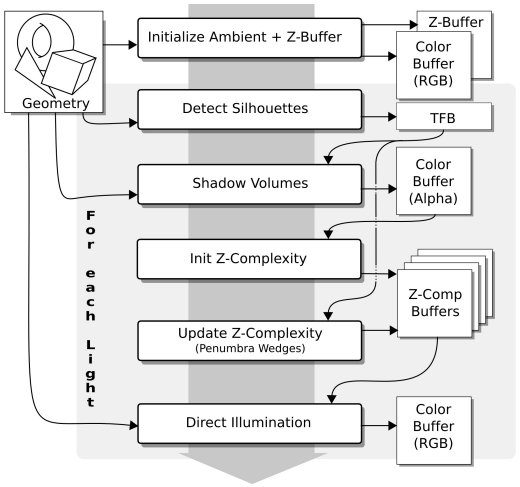


**Figure 6:** *Overview of our algorithm for GPU implementation of the proposed depth complexity evaluation. All computations are performed on the GPU without transferring data to main memory.*

## 7. Implementation

In this section, we present a GPU-intensive implementation of our algorithm. The proposed rendering algorithm (algorithm 2) is developed for the latest generation of graphics hardware. We therefore use *fragment programs* (FP), *vertex programs* (VP) and *geometry programs* (GP). Figure 6 summarizes the GPU implementation and the *render context* organization, which we elaborate in the following explanations.

### 7.1. Sampling Distributions

Depending on the sampling strategy and light type we precompute, and store into textures, the corresponding 2D sample distribution (we assume that omni-directional light sources can be parametrized in 2D). In order to limit the requirements on memory and the number of texture accesses,

**Algorithm 2** render_scene(Scene $w$, RenderView $v$)

```
Require: Pre-computed samples pattern
  set_up_camera(v);
  (color-buffer, z-buffer) ← draw_ambient_lighting(w);
  if Interleaved Sampling then
    init_discontinuity_buffer();
  end if
  for all l ∈ w.lights do
    clear_shadow_buffers();
    E ← silhouette_edges(l, w);
    init_depth_complexity(E);
    if Adaptive sampling then
      define_max_depth_complexity();
    end if
    W_o ← build_outer_wedges(E);
    W_i ← build_inner_wedges(E);
    update_depth_complexity(W_o, W_i);
    if v-buffer is used then
      v-buffer ← v-coef_from_depth_complexity();
      if Interleaved Sampling then
        filter_v-buffer();
      end if
      color-buffer+ =draw_modulated_direct(l, w);
    else
      if Interleaved Sampling then
        color-buffer+ =filter(direct_illumination(l, w));
      else
        color-buffer+ =direct_illumination(l, w);
      end if
    end if
  end for
```

we pack several 2D sample positions per texel. Since the sample positions are computed in the normalized texture space, a precision of *one* byte per coordinate does not introduce a significant error. This precision allows us to encode *two* sample positions in a texture channel of *four*-byte. Hence, using *four* channels (*i.e.* a RGBA texture), we obtain *eight* sample positions in *one* texture fetch. Note that textured lights require the luminance of each sample. Thus, in addition to their packed position, we pre-compute for these lights an $N \times M$ 24-bit RGB texture that stores the $N$ sample luminances for $M$ sets of decorrelated sample patterns.

### 7.2. Soft Shadow Volumes Framework

**Silhouettes detection:** We perform silhouette detection on the GPU using a specific GP. The detected silhouettes are stored on the GPU in a *Transform Feedback Buffer* (TFB). Since writing to the TFB is asynchronous, CPU computations such as scissor rectangle definition or depth bounds evaluation [Len05] are performed in parallel. Note that according to the desired quality and performance trade-off, the silhouette determination can be computed with either accurate or standard detection.

**Shadow volumes:** Silhouette edges are then used in the shadow volume pass to define the initial value of the depth complexity function. We perform silhouette edge extrusion with a GP. In order to avoid a costly access to the stencil buffer, the z-fail stencil test [Car00] is performed in a single pass in a simple FP. The resulting value is then cumulatively blended in the alpha channel of the color buffer:

```
# face.x = fragment is front-facing ? 1 : -1
ATTRIB face = fragment.facing;
ATTRIB fPos = fragment.position;
TEMP r0;

# texture[0] == zBuffer
TEX    r0.x, fPos,     texture[0], RECT;
SGE    r0.x, fPos.z,   r0.x;
MUL    result.color.w, r0.x, -face.x;
```

For a robust z-fail stencil update, the shadow volumes have to be capped. Thus, we use a specific GP to compute the shadow volumes capping in an additional geometric pass.

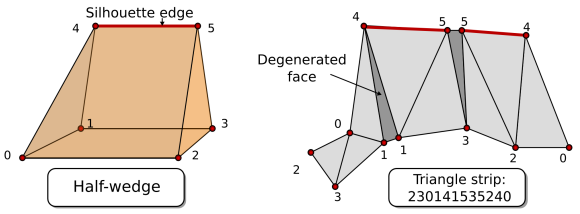


**Figure 7:** *Triangle strip used for the half-wedge generation. This strip implicitly defines coherent normals for each face. Therefore, common optimisations based on the face orientations can be used [Len05].*

**Wedges:** In order to reduce memory consumption, wedges are robustly extruded to infinity during the depth complexity evaluation, rather than being pre-computed and stored. We perform this construction with a GP. However, the performance of a GP is influenced by the number of generated data. Thus, the number of required vertexes is minimized using a single triangle strip per wedge and only *twelve* vertexes per half-wedge. Figure 7 illustrates this generation of wedges. Also, common fill-rate optimisations and fragment rejection are used during the wedges rendering. We refer to [Len05] and [FBP06] for additional details.

### 7.3. The Depth Complexity Computation Step

**Counter packing representation:** Since reading and writing in the same buffer is prohibited, we use the blending operations of the GPU to perform the counter updates. Unfortunately, even though the latest GPUs support integers, their blending is not yet supported. This avoids a naïve GPU implementation of the depth complexity update. On the one hand, the counter packing corresponds to a base decomposition where each base factor encodes the value of a counter with a precision up to the base$-1$ *e.g. two* counters $c_0$ and $c_1 \in [0 \cdot \cdot 255]$ packed in a *two*-byte value $k$ is decomposed in

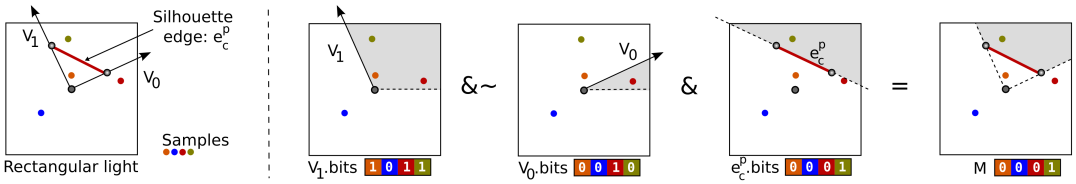


**Figure 8:** *Determination of the samples covered by the projected clipped edge $e_c^p$. A cube map encodes the covered samples from the origin to $v_x$ ($x \in \{0,1\}$) while a 2D texture stores the samples covered by the $e_c^p$ line. The effective covered samples are then simply defined by a logical combination of the fetched bitfields.*

base 256 as $k = c_0 * 256^0 + c_1 * 256^1$. On the other hand the simple precision floating point values are supported for both buffer format and blending operations. With this representation, one can count up to $2^{24} - 1$ without missing an integer value and this value can be expressed in the following base decomposition:

$$2^{24} - 1 = 255 * \left(256^0 + 256^1 + 256^2\right) \quad (7)$$

$$= 63 * \left(64^0 + 64^1 + 64^2 + 64^3\right) \quad (8)$$

$$= 15 * \left(16^0 + 16^1 + 16^2 + 16^3 + 16^4 + 16^5\right) \quad (9)$$

$$= 7 * \left(8^0 + 8^1 + 8^2 + 8^3 + 8^4 + 8^5 + 8^6 + 8^7\right) \quad (10)$$

Thus, we use the floating point representation and the base decompositions exposed in equations 7, 8, 9 and 10, to pack the depth complexity counters.

**Depth complexity initialization:** We present the depth complexity initialization with a fixed Base 64 (B64) counter packing representation (equation 8). A B64 counter packing provides *sixteen* depth complexity counters per 128-bits RGBA buffer. We then use *Multi Render Target* (MRT) to increase the number of counters. Even tough recent GPUs support up to *eight* MRT, we limit the memory bandwidth and its consumption by using at most *four* MRTs (*i.e.* 64 counters). The depth complexity initialization of the 64 counters is then very simply performed via an FP as:

```
ATTRIB fPos = fragment.position;
TEMP r0;

# texture[0].w == stencil value
# 266305 == 64^0 + 64^1 + 64^2 + 64^3
TEX    r0.w, fPos, texture[0], RECT;
MUL    r0.w, r0.w, 266305;
MOV    result.color[0], r0.w;
MOV    result.color[1], r0.w;
MOV    result.color[2], r0.w;
MOV    result.color[3], r0.w;
```

**Depth complexity update:** One of the main challenge we face while updating the depth complexity is efficiently determining samples covered by the projected clipped edge $e_c^p$. Despite having access to *eight* sample positions in one texture fetch, a naïve search leads to a complexity in $O(N)$ where $N$ is the number of samples. We therefore propose an efficient discrete approach to finding the covered samples. A pre-computed 4D texture [AAM03] uses large amount of memory and produces discretization artifacts (figure 9(a)), while the Hough transform, as in [ED07], requires that we either approximate, or pre-compute, the unsupported arc-cosine function. This leads to either additional texture fetches or heavy computation. Hence, we propose a new discrete representation (figures 8 and 9(b)). First, covered samples lying in a sector defined by the origin and vector $v_x$ ($x \in \{0,1\}$) are encoded in a bit field and stored in a cube map. Then, a 2D texture indexed by the orthogonal projection of the light center onto the line $e_c^p$ stores the bit field of samples covered by this line. The final bit mask $M$ is then simply defined as $M = v_1.bits \;\&\; (\sim v_0.bits) \;\&\; e_c^p.bits$. Finally, we iterate through the bits of $M$ to update the corresponding counters. Despite the use of integer operations, which are less efficient than floating point, this method requires only *three* texture fetches and a logical combination to define all the covered samples. Note that this discretization is robust even though the light center passes through the line $e_c^p$. Indeed, in this case, the effective covered samples are just defined by the cube map and so the 2D texture has to store a field of bits set at *one*.

(a) (b) (c)

**Figure 9:** *(a) Illustration of the artifacts introduced by a discretization of the back projected edges and the corresponding covered samples in a $1024 \times 1024$ 4D texture (16 MB). (b) Our discretization using a $64 \times 64 \times 6$ cube map and a $512 \times 512$ 2D texture (4.375 MB). (c) Determination of the covered samples without discretization.*

### 7.4. Rendering the Direct Illumination

Finally, the depth complexities associated with a fragment are used to solve either the equation 6 or to compute the corresponding v-coef (equation 2). The first approach merges the direct illumination computation with the visibility queries while the second performs an additional step to compute the v-coef used to modulate the direct lighting. The resulting lighting contribution is then cumulatively blended. Note that in both cases, the interleaved sampling strategy requires an additional filtering step combining the interleaved sampling patterns [SIMP06].

## 8. Results

### 8.1. Memory Cost

| | | Format | Memory cost |
|---|---|---|---|
| (a) | **Silhouettes TFB** | 1,310,720 × 32F | 5MB |
| (b) | **Samples position** | 64 samples packed in RGBA 32F | 128B |
| (c) | **Edge LUT** | $\left(512^2 + 6 * 64^2\right) *$ RGBA 32F | 4.375MB |
| (d) | **Per light LUT** | 64 × 64 RGB 8UB | 12KB |
| (e) | **Color + Stencil buffer** | RGBA 16F | 8MB |
| (f) | **Z-buffer** | DEPTH_COMPONENT24 | 3MB |
| (g) | **V-buffer** | RGB 8UB | 3MB |
| (h) | **Discontinuity buffer** | Alpha 8UB | 1MB |
| (i) | **Temp filtered buffer** | RGBA 8UB | 4MB |
| (j) | **Deferred buffer** | RGB 32F | 12MB |
| (k) | **DC-buffer(s)** | RGBA 32F | 16MB |

**Table 1:** *Detailed memory costs of our algorithm implementation with a* $1024^2$ *image resolution. An edge LUT (c) stores our discret covered samples representation while a per light LUT (d) stores the luminance texture lookup defined per textured light. The v-buffer (g) is not used when the equation 6 is solved. Finally, discontinuity (h), temp filtered (i) and deferred (j) buffers are only necessary with an interleaved sampling strategy.*

Table 1 shows the memory used by data structures in our implementation. We do not apply any texture compression in order to present significant memory cost without the influence of a specific/subjective compression method. In addition, we reserve 5MB of memory for the silhouettes Transform Feedback Buffer, allowing us to store up to 655,360 silhouette edges.

The memory requirement of our algorithm is *independent* of the scene complexity and depends only on the algorithm parametrization and the light types of the scene. Using only one depth complexity buffer (DC-buffer) for direct illumination without textured light and covered samples discretization requires only $(a)+(b)+(e)+(f)+(k) \approx 32MB$ of memory. On the other hand, computing an image modulated by the v-buffer, with *ten* textured lights, *four* DC-buffers, an interleaved sampling strategy and the discrete covered samples representation requires $(a)+(b)+(c)+10*(d)+(e)+(f)+(g)+(h)+(i)+(j)+4*(k) \approx 105.575MB$ of memory. However, this memory requirement is not a limitation on current high-end GPUs.

### 8.2. Performances

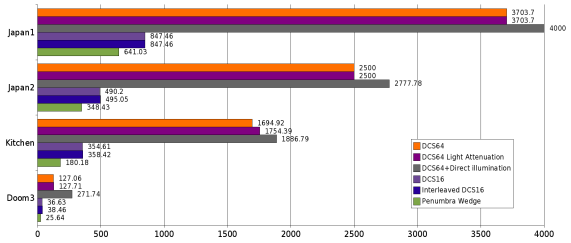


**Figure 10:** *Time in milliseconds of the rendering for a* $1024^2$ *image. Japan1:* 4 *lights,* 501,650 *polygons; Japan2: Japan1 scene with a reduced number of polygons (*246,176 *triangles); Kitchen:* 2 *lights,* 146,131 *polygons; Doom3:* 2 *lights,* 17,693 *polygons.*

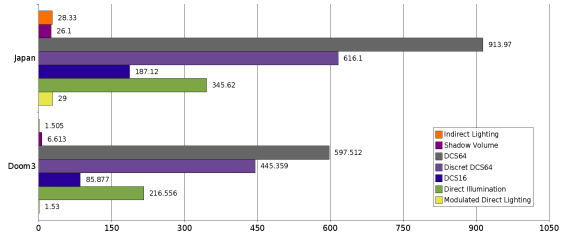


**Figure 11:** *Time in milliseconds of the rendering steps according to the algorithm parametrization. The two test scenes are lit by a single light that generates large penumbra region. Image resolution:* $1024^2$*; Polycount: Japan*=501,650*, Doom3*=17,693

We present the performance on a complete $1024 \times 1024$ image rendering. Indirect lighting is approximated with an irradiance map [RH01] and the Blinn BRDF [Bli77] is used for the materials' appearance. Our renderer is based on the OpenGL API and all the shaders are written in the pseudo assembly language of the NV_gpu_program4 extension. The results are measured on a 64-bits Linux workstation with a Core 2 Duo E6700, 4GB of DDR2 800Mhz and a Geforce 8800GTX. Our benchmarks measure the global rendering time (figure 10) and the cost of the different steps (figure 11) on *three* test scenes (figure 12) with varying algorithm parametrization. To stress our approach, the light sources are not attenuated and so they do not take advantage of per-light scissor and depth bound optimisations. Finally, we use a counter packing representation where each DC-buffer stores 16 depth complexity counters with a precision up to 63 (equation 7).

Figure 10 illustrates that the Depth Complexity Sampling with 16 samples (DCS16) is approximately 5 times faster than using 64 samples (DCS64). This performance improvement is explained by the limitation on memory bandwidth and texture fetches, in addition of the reduction in working

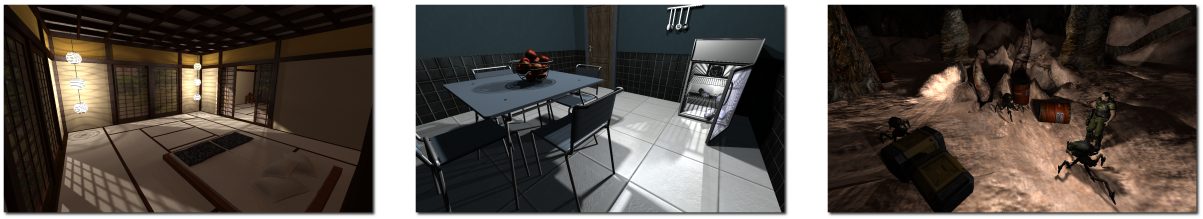

(a) Japan (b) Kitchen (c) Doom3

**Figure 12:** *The three test scenes used in our benchmark. (a) and (b) are high-polygon scenes while (c) is a game scene including animated skinned characters.*

load of the raster operation unit. To reduce the noise of the shadows computed with 16 depth complexity counters, the interleaved sampling strategy can be used with a negligible performance cost. Computing shadows for semi-opaque occluders is less than 4% slower than the common depth complexity sampling. Note that compared to a direct lighting modulated by a v-buffer, solving the equation 6 leads to a performance drop between 8% and 12%, except for the game scene, where the rendering time is multiplied by more than 2. This result is explained by the effectiveness of the v-buffer on low-polygon scenes. Indeed, in these scenes the simple direct lighting computation step is very fast, since very few triangles have to be transformed. However, solving the equation 6 is more computationally intensive and results in a more important performance gap between the two direct lighting approaches than on a high-polygon scene (figure 11). Finally, we observe in figure 11 that our discrete covered samples representation improves performance by a percentage between 25% and 33% with respect to a naïve search of the covered samples.

## 9. Discussion and Future Works

The presented depth complexity sampling algorithm allows the generation of fast and accurate shadows. However, since it uses the soft shadow volume framework, it handles only polygonal models and is submitted to fill-rate bottleneck. Furthermore, the splitting of wedges in inner and outer parts generates aliasing due to precision errors. Nevertheless, our approach is orthogonal to the previous object-based methods and thus it may take advantage of all their current and future improvements.

Due to its sampling nature, and despite the use of the adaptive sampling strategy, the proposed algorithm is still exposed to the sub-sampling artifacts. However, since we use a Monte Carlo sample distribution, averaging the result of several runs would give a solution that would be statistically very close to the exact solution. One can therefore imagine a progressive rendering or a multi-GPU system where each picture is computed according to different sampling distribution and then averaged in the final image.

The adaptive sampling algorithm defines the counter packing representation for a given point of view. Note that the counter packing encoding can be locally defined per pixel rather than globally set for the current rendered image. A simple idea is to track the number of wedges bounding each pixel.

The lack of integer support in the blending stage limits both the precision of the counters and the efficiency of memory usage. In addition, despite the use of an adaptive sampling strategy, the counter packing robustness is still compromised by an eventual overflow error. We propose an API extension that address these limitations by exposing a buffer as a pool of $m$ available bits for each pixel. The application would explicitly define how to partition $m$ into $N$ channels, while a pool of bits would be reserved to save the state of each channel (overflow error, `NaN` indicator *etc.*).

(a) pWedge (b) DCS (c) RT

**Figure 13:** *Comparison of the shadows generated by the penumbra wedge algorithm (a), our Depth Complexity Sampling (b) and a Ray-Traced reference (c). In addition of the overlapping penumbrae artifact, the penumbra wedge algorithm produces an incorrect lighting due to the single light sample direct lighting computation.*

## 10. Conclusion

We have presented an accurate and efficient soft shadow volume algorithm based on a new fast evaluation of the depth complexity function. The proposed algorithm addresses the limitations of both the penumbra wedge approach [AAM03] (figure 13) and the offline soft shadow volume methods [LAA*05, LLA06]. We have demonstrated that, despite its

object-based nature, this algorithm can efficiently deal with complex animated models lit by a complex direct illumination. Contrary to the image-based approaches, our method does not use a discrete, surjective scene representation. In addition it naturally handles the omni-directional surfacic lights without any additional drop in performance or specific treatments.


### Acknowledgements

We thank Tom Cashman for his help in the completion of the paper.


### References


[AAM03] ASSARSSON U., AKENINE-MÖLLER T.: A geometry-based soft shadow volume algorithm using graphics hardware. *ACM Transactions on Graphics, Proc. SIGGRAPH 22*, 3 (2003), 511–520.

[AHL*06] ATTY L., HOLZSCHUCH N., LAPIERRE M., HASENFRATZ J.-M., HANSEN C., SILLION F.: Soft shadow maps: Efficient sampling of light source visibility. *Computer Graphics Forum 25*, 4 (2006), 725–741.

[AHT04] ARVO J., HIRVIKORPI M., TYYSTJÄRVI J.: Approximate soft shadows with an image-space flood-fill algorithm. *Computer Graphics Forum, Proc. EUROGRAPHICS 23*, 3 (2004), 271–280.

[AMA02] AKENINE-MÖLLER T., ASSARSSON U.: Approximate soft shadows on arbitrary surfaces using penumbra wedges. In *Proc. EG Workshop on Rendering Techniques* (2002), Eurographics, pp. 297–306.

[ARHM00] AGRAWALA M., RAMAMOORTHI R., HEIRICH A., MOLL L.: Efficient image-based methods for rendering soft shadows. In *Proc. SIGGRAPH* (2000), ACM Press, pp. 375–384.

[ASK06] ASZÓDI B., SZIRMAY-KALOS L.: Real-time soft shadows with shadow accumulation. In *EUROGRAPHICS short papers* (2006).

[BCS06] BAVOIL L., CALLAHAN S. P., SILVA C. T.: *Robust Soft Shadow Mapping with Depth Peeling*. Tech. Rep. UUSCI-2006-028, University of Utah, 2006.

[Bli77] BLINN J. F.: Models of light reflection for computer synthesized pictures. In *Proc. SIGGRAPH* (1977), ACM Press, pp. 192–198.

[BS02] BRABEC S., SEIDEL H.-P.: Single sample soft shadows using depth maps. In *Proc. Graphics Interface* (2002), pp. 219–228.

[Car00] CARMACK J.: Email to private list. Id-Software, 2000.

[Cro77] CROW F. C.: Shadow algorithms for computer graphics. In *Proc. SIGGRAPH* (1977), ACM Press, pp. 242–248.

[DF94] DRETTAKIS G., FIUME E.: A fast shadow algorithm for area light sources using backprojection. *Computer Graphics Forum 28* (1994), 223–230.

[ED06] EISEMANN E., DÉCORET X.: Plausible image based soft shadows using occlusion textures. In *Proc. of the Brazilian Symposium on Computer Graphics and Image Processing* (2006), Conference Series, IEEE Computer Society, pp. 155–162.

[ED07] EISEMANN E., DÉCORET X.: Visibility sampling on gpu and applications. *Computer Graphics Forum, Proc. EUROGRAPHICS 26*, 3 (2007), 535–544.

[FBP06] FOREST V., BARTHE L., PAULIN M.: Realistic soft shadows by penumbra-wedges blending. In *Proc. SIGGRAPH/EUROGRAPHICS conference on Graphics hardware* (2006), Eurographics, pp. 39–48.

[Fer05] FERNANDO R.: Percentage-closer soft shadows. In *SIGGRAPH Sketches* (2005), ACM Press, p. 35.

[GBP06] GUENNEBAUD G., BARTHE L., PAULIN M.: Real-time soft shadow mapping by backprojection. In *Proc. EG Symposium on Rendering* (http://www.eg.org/, 2006), Eurographics, pp. 227–234.

[GBP07] GUENNEBAUD G., BARTHE L., PAULIN M.: High-quality adaptive soft shadow mapping. *Computer Graphics Forum, Proc. EUROGRAPHICS 26*, 3 (2007), 525–533.

[HBS00] HEIDRICH W., BRABEC S., SEIDEL H.-P.: Soft shadow maps for linear lights. In *Proc. EG Workshop on Rendering Techniques* (2000), Eurographics, pp. 269–280.

[HLHS03] HASENFRATZ J.-M., LAPIERRE M., HOLZSCHUCH N., SILLION F.: A survey of real-time soft shadows algorithms. In *State-of-the-Art Report, Proc. EUROGRAPHICS* (2003), Eurographics.

[Kaj86] KAJIYA J. T.: The rendering equation. In *Proc. SIGGRAPH* (1986), ACM Press, pp. 143–150.

[KH01] KELLER A., HEIDRICH W.: Interleaved sampling. In *Proceedings of the 12th Eurographics Workshop on Rendering Techniques* (2001), Eurographics, pp. 269–276.

[LAA*05] LAINE S., AILA T., ASSARSSON U., LEHTINEN J., AKENINE-MÖLLER T.: Soft shadow volumes for ray tracing. *ACM Transactions on Graphics, Proc. SIGGRAPH 24*, 3 (2005), 1156–1165.

[Len05] LENGYEL E.: Advanced stencil shadow and penumbra wedge rendering. Game developer Conference, unpublished slides, 2005.

[LLA06] LEHTINEN J., LAINE S., AILA T.: An improved physically-based soft shadow volume algorithm. *Computer Graphics Forum, Proc. EUROGRAPHICS 25*, 3 (2006), 303–312.

[PH04] PHARR M., HUMPHREYS G.: *Physically Based Rendering: From Theory to Practice*. Morgan Kaufmann, 2004, ch. Monte Carlo Integration I: Basic Concepts, pp. 631–660.

[RH01] RAMAMOORTHI R., HANRAHAN P.: An efficient representation for irradiance environment maps. In *Proc. SIGGRAPH* (2001), ACM Press, pp. 497–500.

[RSC87] REEVES W. T., SALESIN D. H., COOK R. L.: Rendering antialiased shadows with depth maps. *Proc. SIGGRAPH 21*, 4 (1987), 283–291.

[SAPP05] ST-AMOUR J.-F., PAQUETTE E., POULIN P.: Soft shadows from extended light sources with penumbra deep shadow maps. In *Proc. of Graphics Interface* (2005), pp. 105–112.

[SIMP06] SEGOVIA B., IEHL J.-C., MITANCHEY R., PÉROCHE B.: Non-interleaved deferred shading of interleaved sample patterns. In *Proc. SIGGRAPH/EUROGRAPHICS conference on Graphics hardware* (2006), Eurographics, pp. 53–60.

[SS98] SOLER C., SILLION F.: Fast calculation of soft shadow textures using convolution. In *Proc. SIGGRAPH* (1998), ACM Press, pp. 321–332.

[SS07] SCHWARZ M., STAMMINGER M.: Bitmask soft shadow. *Computer Graphics Forum, Proc. EUROGRAPHICS 26*, 3 (2007), 515–524.

[Wil78] WILLIAMS L.: Casting curved shadows on curved surfaces. In *Proc. SIGGRAPH* (1978), ACM Press, pp. 270–274.

[WPF90] WOO A., POULIN P., FOURNIER A.: A survey of shadow algorithms. *IEEE Compututer Graphics Application 10*, 6 (1990), 13–32.